Europium doping in monoclinic $KYb(WO_4)_2$ crystal

P.A. Loiko[1,2], E.V. Vilejshikova[2], X. Mateos[1,*], J.M. Serres[1], E.B. Dunina,[3] A.A. Kornienko,[3] K.V. Yumashev[2], M. Aguiló[1] and F. Díaz[1]

[1]*Física i Cristal·lografia de Materials i Nanomaterials (FiCMA-FiCNA), Universitat Rovira i Virgili (URV), Campus Sescelades, c/ Marcel·lí Domingo, s/n., Tarragona, Spain E-43007*
[2]*Center for Optical Materials and Technologies (COMT), Belarusian National Technical University, 65/17 Nezavisimosti Ave., Minsk 220013, Belarus*
[3]*Vitebsk State Technological University, 72 Moskovskaya Ave., Vitebsk, Belarus 210035*

*Corresponding author, e-mail: xavier.mateos@urv.cat

Abstract We report on a detailed spectroscopic study of Eu^{3+} ions in the monoclinic $KYb(WO_4)_2$ crystal. The polarized room and low-temperature absorption spectra are measured. The maximum σ_{abs} corresponding to the $^7F_1 \rightarrow {}^5D_1$ transition is 1.32×10^{-20} cm^2 at 534.2 nm with a bandwidth of 0.7 nm (for $E \parallel N_m$). The Stark sub-levels of the excited mulitplets are determined. A Judd-Ofelt analysis is applied to the Eu^{3+}:$KYb(WO_4)_2$ crystal to determine the probability of spontaneous transitions, radiative lifetimes and luminescence branching ratios. Within the strong configuration interaction (SCI) approximation, the intensity parameters are Ω_2 = 4.757, Ω_4 = 2.295, Ω_6 = 1.644 [10^{-20} cm^2] and Δ_f = 50160 cm^{-1}. The radiative lifetime of the $^5D_0$ state is 351 μs. The maximum stimulated-emission cross-section corresponding to the $^7F_1 \rightarrow {}^5D_1$ transition is 1.44×10^{-20} cm^2 at 703.2 nm (for $E \parallel N_m$). Under UV excitation, the Eu^{3+}: $KYb(WO_4)_2$ crystal provides intense red photoluminescence with CIE coordinates, x = 0.675, y = 0.325.

Keywords: double tungstates, europium, absorption, luminescence.

1. Introduction

During the last decade, the interest to rare-earth lasers emitting in the visible has gradually increased. A clear example are those based on Praseodymium (Pr^{3+}) which can generate multi-color output in the green, yellow and red spectral regions [1,2] due to the multiple transitions from the metastable $^3P_0$ state. Such lasers are wavelength-tunable [3] and power scalable [4]. Laser operation of Terbium (Tb^{3+}), Samarium (Sm^{3+}) and Dysprosium (Dy^{3+}) [5,6] in the visible has been recently reported. Visible lasers have potential applications in color displays, data storage, holography, spectroscopy and medicine. To a great extent, the success in the development of novel visible lasers was due to the search of appropriate hosts for the active ions.

Trivalent Europium (Eu^{3+}) is another ion that is very suitable for obtaining visible emissions (red and deep-red). Such multiple transitions are from the metastable $^5D_0$ state to lower-lying ^7F_J (J = 0...6) multiplets. Spectrally, they cover the ~590 to 800 nm range. The typical lifetime of the $^5D_0$ state of Eu^{3+} is ~0.1-1 ms and the luminescence quantum efficiency from this state approaches unity (separated by an energy gap of ~12000 cm^{-1} from the lower lying state). Red phosphors based on Eu^{3+} ions like the commercial yttrium oxide, Eu:Y_2O_3 [7], are used in tricolor lamps, field emission displays, cathode-ray tubes and solid-state lighting. Eu^{3+} ions are also suitable for laser operation on the $^5D_0 \rightarrow {}^7F_2$ (at ~610 nm) [8,9] and $^5D_0 \rightarrow {}^7F_4$ (at ~702 nm) [10] transitions.

Recently, monoclinic double tungstate (DT) crystals with a general chemical formula $KRE(WO_4)_2$ or shortly KREW where RE = Gd, Y, Lu, Yb, etc. were found to be very suitable for Eu^{3+} doping and room-temperature laser operation at ~702 nm in the deep-red spectral region was demonstrated [11]. DT are well-known materials for rare-earth doping [12] and efficient lasers were previously realized with Yb^{3+} [13], Tm^{3+} [14] and Ho^{3+} [15] ions. As for Eu^{3+}, DTs offer large polarized transition cross-sections, possibility of high doping levels (up to 25 at.% with some hosts) accompanied with a weak luminescence quenching and no $Eu^{3+} \rightarrow Eu^{2+}$ reduction [16,17]. Laser operation of Eu in KGdW [18] and KYW [19] has been reported. The spectroscopy of Eu:KREW crystals with RE = Gd [11], Y [17] and Lu [16,20,21] is also known. Nanocrystalline phosphors based on Eu:DTs have shown intense red photoluminescence [22-26].

There is a fourth representative of the DT family, the potassium ytterbium double tungstate or KYbW. This crystal can be grown with a good optical quality [27] and it is also suitable for Eu^{3+} doping. Indeed, the ionic radii of the VIII-fold coordinated Yb^{3+} and Eu^{3+} are 0.985 Å and 1.066 Å, respectively, which is even closer than for the Lu^{3+} (0.977 Å) and Eu^{3+} ions in Eu:KLuW. In the present paper, we perform a detailed study of the spectroscopic properties of the Eu:KYbW crystal from the point of view of its potential laser applications. Such a characterization involves the Judd-Ofelt modeling, the refinement of the Stark splitting and the calculation of the transition cross-sections. A previous study of bulk Eu:KYbW focused mainly on cooperative emissions [28,29], while the study of nanocrystalline Eu:KYbW [24] evaluated its potential as red phosphor.

2. Crystal growth

A monoclinic (space group C^6_{2h} – *C2/c*) Eu^{3+}:$KYb(WO_4)_2$ (Eu:KYbW) single crystal was grown by the Top Seeded Solution Growth (TSSG) Slow-Cooling method using potassium ditungstate, $K_2W_2O_7$, as a solvent. The solution mixture (11.5 mol% KYbW as a solute – 88.5 mol% $K_2W_2O_7$ as a solvent), 50 g in weight was introduced into a vertical tubular furnace using a 25 cm^3 conical platinum crucible. The starting materials, K_2CO_3, Yb_2O_3, Eu_2O_3 and WO_3 were from Aldrich and Fluka (>99.9% purity). The concentration of Eu in the solution was 1 at.%. The solution was homogenized at 50 K above the saturation temperature for ~6 h. The saturation temperature at the above mentioned particular solute/solvent ratio was 1170–1175 K. The thermal gradient in the solution corresponding to the axial direction was ~1 K/cm; the bottom being hotter than the surface of the solution. A seed from an undoped KYW was oriented with its crystallographic *b*-axis perpendicular to the solution surface. The solution temperature was decreased by ~20 K at a rate of 0.1 K/h. The seed was rotated at 40 rpm (without pulling). After 8–10 days of crystal growth, the crystal was slowly removed from the solution at a rate of 1 mm per 10 min and after the grown crystal lost contact with the solution, the furnace was cooled down to room temperature at 25 K/h to avoid thermal shocks. The as-grown crack- and inclusion-free crystal was of high optical quality and had a slight rose coloration due to the Eu, Fig. 1. The actual Eu^{3+} ion density in the grown crystal N_{Eu} =0.64×10^{-20} cm^{-3} was measured using Electron Probe Micro Analysis (EPMA). The segregation coefficient for Eu^{3+} ions was close to unity. The stoichiometric crystal composition was $KYb_{0.99}Eu_{0.01}(WO_4)_2$.

3. Experimental

Eu:KYbW is a biaxial crystal [12]. Its optical properties are described within the frame of the optical indicatrix with the principal axes N_p, N_m and N_g. The N_p-axis is parallel to the *b* crystallographic axis and the two remaining ones are located in the *a-c* plane, N_m^a = 59.7° and N_g^c = 19° [27]. For the spectroscopic studies, the sample was cut from the as-grown bulk in the optical indicatrix frame having the dimensions ~3(*p*)×3(*m*)×3(*g*) mm^3 and it was polished from all sides.

The room-temperature (RT, 293 K) absorption spectrum of Eu:KYbW was measured with a Varian CARY-5000 spectrophotometer. In the visible (300...650 nm), the spectral bandwidth (SBW) was 0.01 nm and in the near-IR (1.8...2.8 μm), the SBW = 0.1 nm. The absorption cross-section was calculated from the absorption coefficient, $\sigma_{abs} = \alpha/N_{Eu}$. For low-temperature (LT) measurements at 6 K, we used an Oxford Instruments Ltd. cryostat (SU 12 model) with helium-gas close-cycle flow.

The photoluminescence (PL) of Eu:KYbW was excited at 400 nm by a blue GaN diode. The spectrum was measured with a lock-in amplifier, a monochromator MDR-23 (SBW <0.1 nm) and a sensitive Hamamatsu C5460-01 photodetector. A Glan-Taylor prism was used for the emission to separate the N_p, N_m and N_g polarizations. The spectral sensitivity of the set-up was determined with a halogen lamp with a calibrated spectral power density.

For the luminescence decay studies, a nanosecond (ns) optical parametric oscillator Lotis TII LT-2214 tuned to 534 nm was used as excitation source. The decay curves were detected with a monochromator MDR-12 (SBW ~1 nm), a fast Hamamatsu C5460

photodetector (response time, 40 ns) and a 500 MHz Textronix TDS-3052B digital oscilloscope. The decay from the $^5D_0$ state was monitored at 610 nm and 702 nm, and the characteristic decay time τ was determined according to a single-exponential law, $I_{PL} = I_0 \exp(-t/\tau)$.

The Raman spectra were measured with polarized light using a Renishaw inVia Raman microscope with a x50 objective and the spectral resolution was ~0.1 cm^{-1}. The excitation was by a He-Ne laser at 632.8 nm.

4. Results and Discussion

4.1 Optical Absorption

The optical absorption spectrum of the Eu:KYbW crystal is shown in Fig. 2 (for light polarization $E \parallel N_m$, at RT). The feature of Eu^{3+} is a small energy gap between the ground state ($^7F_0$) and the lower-lying excited state ($^7F_1$), ~300 cm^{-1}. The latter manifold is efficiently thermally populated at RT (the fractional populations for $^7F_0$, $^7F_1$ and $^7F_2$ states estimated from a Boltzmann distribution are ~0.65, 0.33 and 0.02, respectively). In the absorption spectrum of Eu:KYbW, the transitions from the $^7F_0$ and $^7F_1$ states to the higher-lying multiplets are detected. In the near-IR, the characteristic bands of Eu^{3+} related to the transitions $^7F_{0,1} \rightarrow {}^7F_5$ (~2600 nm) and $^7F_6$ (~2060 nm) are observed. In the visible, well-resolved absorption bands are related to the transitions to the $^5D_0$ (~590 nm), $^5D_1$ (~530 nm), $^5D_2$ (~465 nm), $^5D_3$ (~410 nm) and $^5L_6$ excited-states (~396 nm). At shorter wavelength, the absorption is related to the transitions to $^5L_{7,8}$, $^5G_{2\text{-}6}$ and $^5D_4$ multiplets for which individual Stark levels can overlap and making the assignment of the bands very complicate. The UV absorption edge for Eu:KYbW crystal is at ~320 nm (E_g ~3.9 eV).

The irradiation of Eu:DTs with a high-power UV laser can lead to the formation of color centers and crystal darkening that prevents the laser operation [18]. The excitation of Eu:KYbW with mJ-level ns pulses at 355 nm resulted in a persistent darkening of the crystal. The inspection of the absorption spectrum revealed weak (α_{abs} < 0.1 cm^{-1}) absorption band spanning from ~400 to 500 nm. Thus, we will discuss only the absorption bands in the visible that can be used to pump the Eu:KYbW crystal.

The anisotropy of the optical absorption of Eu:KYbW related to the transitions $^7F_{0,1} \rightarrow {}^5L_6$, $^7F_0 \rightarrow {}^5D_2$ (in the blue region) and $^7F_{0,1} \rightarrow {}^5D_1$ (green region) is analyzed in Fig. 3 for the principal light polarizations. As previously determined for other rare-earth-doped DTs, Eu:KYbW is characterized by a strong anisotropy of the absorption. The strongest absorption corresponds to light polarization $E \parallel N_m$, for $E \parallel N_p$ it takes an intermediate place, while $E \parallel N_g$ is almost not suitable for pumping.

A very intense band centered at 394.9 nm ($\sigma_{abs} = 16.1\times10^{-20}$ cm^2, full width at half maximum, FWHM <0.3 nm, for $E \parallel N_m$) is atributed to the $^7F_0 \rightarrow {}^5L_6$ transition. It can be used for pumping of Eu:KYbW by blue GaN diodes emitting at ~400 nm. A second intense absorption band in the blue contains two very narrow (FWHM <0.15 nm) peaks at 465.2 and 466.6 nm ($E \parallel N_m$), and one peak at 466.0 nm ($E \parallel N_p$). The maximum σ_{abs} corresponding to $E \parallel N_m$ is 9.2×10^{-20} cm^2. Eu:KYbW can be pumped into this band by a frequency-doubled optically pumped semiconductror laser (OPSL).

The band related to the $^7F_1 \rightarrow {}^5D_1$ transition was previously used for pumping of Eu:DTs with green frequency-doubled Nd:KGdW lasers [18,19]. The details about this band (position of the local peaks and the corresponding σ_{abs}) for Eu:KYbW are summarized in Table 1. The maximum absorption cross-section, $\sigma_{abs} = 1.32\times10^{-20}$ cm^2 at 534.2 nm corresponds to $E \parallel N_m$ (with FWHM ~0.7 nm). To show the anisotropy of the absorption in the Eu:KYbW crystal, we calculate the ratio of the absorption cross-sections, $\sigma_{abs}(m):\sigma_{abs}(p):\sigma_{abs}(g)$ at 534.2 nm, that amounts to 5.7:1.6:1. Thus, to provide a high absorption efficiency, the Eu:KYbW laser element should provide access to the $E \parallel N_m$. A much weaker band related to the $^7F_0 \rightarrow {}^5D_1$ transition contains two peaks at 526.9 and 527.9 nm with σ_{abs} ~0.5×10^{-20} cm^2 showing small FWHM, <0.1 nm.

The absorption oscillator strengths for Eu^{3+} ions in KYbW have been determined from the measured absorption spectrum:

$$f_{\Sigma}^{exp}(JJ') = \frac{m_e c^2}{\pi e^2 N_{Eu}^{*} \langle\lambda\rangle^2}\Gamma(JJ'), \tag{1}$$

where m_e and e are the electron mass and charge, respectively, c is the speed of light, N^*_{Eu} is the effective population of the initial state ($^7F_1$ or $^7F_2$) in agreement with the above mentioned Boltzmann factor, $\Gamma(JJ')$ is the integrated absorption coefficient within the absorption band and $\langle\lambda\rangle$ is the "center of gravity" of the absorption band:

$$\Gamma(JJ') = \int \alpha(\lambda) d\lambda, \tag{2a}$$

$$\langle\lambda\rangle = \frac{\int \lambda\alpha(\lambda) d\lambda}{\int \alpha(\lambda) d\lambda}. \tag{2b}$$

Here and further in the Judd-Ofelt modeling, we consider all values as averaged over the three principal light polarizations, e.g. $\langle f\rangle = 1/3(f_p + f_m + f_g)$. The obtained results are summarized in Table 2.

The absorption oscillator strengths can also be determined within the Judd-Ofelt (J-O) theory from the line strengths:

$$f_{ED}^{calc}(JJ') = \frac{8}{3h(2J'+1)\langle\lambda\rangle}\frac{(n^2+2)^2}{9n} S_{ED}^{calc}(JJ'), \tag{3a}$$

$$f_{\Sigma}^{calc}(JJ') = f_{ED}^{calc}(JJ') + f_{MD}(JJ'). \tag{3b}$$

Here, h is the Planck constant and n is the refractive index of the crystal. As known, the Judd-Ofelt theory describes electric-dipole (ED) transitions. The contribution of magnetic-dipole (MD) transitions with J–J' = 0, ±1 can be calculated separately within the Russell-Saunders approximation on wave functions of Eu^{3+} ion under the assumption of a free-ion. The ED line strengths within the conventional J-O theory are expressed as [30,31]:

$$S_{ED}^{calc}(JJ') = \sum_{k=2,4,6} U^{(t)}\Omega_t, \tag{4a}$$

$$U^{(t)} = \langle (4f^n)SLJ \| U^t \| (4f^n)S'L'J' \rangle^2. \tag{4b}$$

Here, $U^{(t)}$ are the squared reduced matrix elements which can be found in the literature and Ω_2, Ω_4 and Ω_6 are the intensity parameters (J-O parameters).

For Eu^{3+} ions in DT crystals, a much better correspondence between the experimental and theoretical oscillator strengths is observed for a modification of the J-O theory for the case of anomalously strong configuration interaction (ASCI) [17,20]. However, the ASCI theory contains 9 fitting parameters [32]. This number is higher than the number of considered absorption bands for Eu:KYbW (N = 8, cf. Table 2). Consequently, a simplified approximation, called strong configuration interaction (SCI), can be applied [33,34]. The computational scheme developed by Judd and Ofelt corresponds to the second order of the Perturbation theory in terms of the energies of virtual transitions of a 4f electron to the states with an opposite parity (5d, 6s). Both ASCI and SCI models refine this scheme by incorporating the third-order perturbative effects. In the SCI model, it is assumed that the excited configurations have the same average energy Δ. The corresponding formula for ED line strengths is [34]:

$$S_{ED}^{calc}(JJ')=\frac{1}{4}\sum_{k=2,4,6}U^{(k)}\Omega_k\left(\frac{\Delta}{\Delta-E_J}+\frac{\Delta}{\Delta-E_{J'}}\right)^2. \quad (5)$$

The root mean square (RMS) deviation between the experimental and calculated absorption oscillator strengths, which is the criterion of the goodness of the modeling, is (N = 8 is the number of fitted transitions):

$$RMS=\sqrt{\frac{\sum(f_{ED}^{\exp}-f_{ED}^{calc})^2}{N-3}} \quad (6)$$

The calculated absorption oscillator strengths for Eu:KYbW are summarized in Table 2 for both J-O and SCI theories. The latter provides much lower RMS deviation of 0.115 (as compared with the conventional J-O theory with RMS = 0.879). The best-fit parameters of both theories are presented in Table 3. In particular, for the SCI theory, Ω_2 = 4.757, Ω_4 = 2.295, Ω_6 = 1.644 [10^{-20} cm^2] and Δ_f = 50160 cm^{-1}.

In order to determine the energy of the Stark sub-levels of the multiplets of Eu^{3+} ions in KYbW, we have performed low-temperature (6 K) absorption measurements. Eu^{3+} has an even number of active electrons, $4f^6$, and in the KYbW crystal it is located in the C_2 site (when substituting Yb^{3+} ions). The ground-state of Eu^{3+}, $^5D_0$, has one Stark level which corresponds to the irreducible representation Γ_1. Thus, at low temperature, only transitions from this level will be observed and the position of peaks will indicate directly the energies of the Stark sub-levels of the excited multiplets. The polarization-dependent selection rules for these transitions [35] are shown in Table 4. As one can see, the $E \parallel N_p$ and $E \parallel N_m$ (N_g) polarizations are distinct. This difference is characteristic of monoclinic *2/m* crystals because the N_p axis is parallel to the two-fold axis C_2 and N_m and N_g axes are positioned in the orthogonal plane.The low-temperature polarized absorption spectra corresponding to the transitions to $^7F_6$, $^5D_0$, $^5D_1$, $^5D_2$, $^5D_3$ and $^5L_6$ excited-states are shown in Fig. 4. The determined energies of the Stark sub-levels and the total theoretical number of sub-levels, $n\Gamma_1 + m\Gamma_2$, are presented in Table 5. The metastable $^5D_0$ state of Eu^{3+} has only one Stark sub-level (Γ_1). The transition $^7F_0 \rightarrow {}^5D_0$ ($\Gamma_1 \rightarrow \Gamma_1$) can be observed only for light polarization $E \parallel N_p$ which agrees with the experimental data, see Fig. 4. The energy of the $^5D_0$ state is 17198 cm^{-1}. The single peak observed for $^7F_0 \rightarrow {}^5D_0$ transitions confirms that there is only one site (C_2) for Eu^{3+} ions in KYbW. As far as we know, this is the first report on the Stark splitting of Eu^{3+} in KYbW.

4.2 Optical Emission

The probability of spontaneous radiative ED transitions is calculated from the corresponding line strengths which are derived from the J-O or SCI parameters and squared reduced matrix elements $U^{(k)}$:

$$A_{ED}^{calc}(JJ')=\frac{64\pi^4 e^2}{3h(2J'+1)\langle\lambda\rangle^3} n\left(\frac{n^2+2}{3}\right)^2 S_{ED}^{calc}(JJ'). \quad (7)$$

The set of $U^{(k)}$ for emission transitions can be found in the literature. Then, all the probabilities are determined by adding the MD contributions (see [36] for the A_{MD} values):

$$A_{\Sigma}^{calc}(JJ')=A_{ED}^{calc}(JJ')+A_{MD}(JJ'). \quad (8)$$

On the basis of the probability of spontaneous transitions for separate emission channels J→J', we have calculated the total probability A_{tot}, the corresponding radiative lifetimes of the excited-states τ_{rad} and luminescence branching ratios for the emission channels B(JJ'):

$$A_{tot}^{calc}=\sum_{J'} A_{\Sigma}^{calc}(JJ'), \quad (9a)$$

$$\tau_{rad}=\frac{1}{A_{tot}^{calc}}, \quad (9b)$$

$$B(JJ')=\frac{A_{\Sigma}^{calc}(JJ')}{\sum_{J'} A_{\Sigma}^{calc}(JJ')} \quad (9c)$$

The results are presented in Table 6 for the excited states $^5D_0$, $^5D_1$, $^5D_2$ and $^5D_3$. On the basis of multiplet energies for the Eu^{3+} free-ion [37], we have also determined the mean emission wavelengths for each J→J' transition, ‹λ›. In the following we discuss the transitions from the metastable $^5D_0$ state. Both ED and MD transitions from $^5D_0$ to $^7F_0$ state are forbidden in agreement with the Wigner-Eckart theorem (as J = J' = 0). The observation of this transition may be due to the effect of the J–J-mixing in the local field that can not be taken into account for the utilized theories. For the $^5D_0 \rightarrow {}^7F_1$ transition, the values of the total angular momentum quantum numbers are J = 0 and J' = 1. In agreement with the Wigner-Eckart theorem, the possible k indices defining the intensity parameters Ω_k, satisfy the relation $|J-J'| \le k \le J+J'$. In other words, k = 1, so that the oscillator strength for the ED transition is defined solely by Ω_1. This parameter is zero for the J-O theory (as well as the SCI one). Thus, the value of $A_{ED}(^5D_0 \rightarrow {}^7F_1)$ is zero (purely MD transition). Similarly, for the $^5D_0 \rightarrow {}^7F_3$ and $^5D_0 \rightarrow {}^7F_5$ ED transitions, k = 3 and 5 ($\Omega_3 = \Omega_5 = 0$), so the corresponding A_{ED} are also zero. Finally, the luminescence branching ratios for the transitions from $^5D_0$ to $^7F_1$, $^7F_2$ and $^7F_4$ states are 3.4%, 86.1% and 10.1%, respectively. The radiative lifetime of the metastable $^5D_0$ state is 351 μs (SCI theory) which is close to the value predicted by the J-O theory, 329 μs, Table 7. The radiative lifetime of the $^5D_0$ state for Eu:KYbW is shorter than for other monoclinic DTs, Eu:KREW with RE = Gd, Y and Lu (450–510 μs) [11,17,20].

The PL spectrum of the Eu:KYbW crystal under UV excitation at ~400 nm (to the $^5L_6$ state) is shown in Fig. 5 (with non-polarized light). The observed emissions are related to the $^5D_J \rightarrow {}^7F_{J'}$ transitions (shortly denoted as J→J'). The PL that occurs from the metastable $^5D_0$

state dominates in the spectrum; the radiative transitions to ^7F_J (J = 1–6) multiplets are detected at ~590 (0→1'), 612 (0→2', the most intense), 650 (0→3'), 703 (0→4'), 740 (0→5') and 810 nm (0→6'). Based on the mean emission wavelength and luminescence branching ratios for luminescence from the higher-lying $^5D_1$, $^5D_2$ and $^5D_3$ excited-states, we interpret a weak Eu^{3+} emission that fall into the blue and green spectral regions, Fig. 5. It should be noted that the spectral position and relative intensities of these emission are in excellent agreement with the theoretical prediction, Table 6.

Eu^{3+} is known for its hyper-sensitive purely ED transition $^5D_0 \rightarrow {}^7F_2$ that is the indicator of the symmetry of the ion site [38]. If the site has no inversion center, this transition will be dominant over the $^5D_0 \rightarrow {}^7F_1$ purely MD transition. The ratio of the integral intensities of the corresponding emission bands is called the asymmetry parameter *R*:

$$R = \frac{I_{\mathrm{ED}}(^5D_0 \rightarrow {}^7F_2)}{I_{\mathrm{MD}}(^5D_0 \rightarrow {}^7F_1)}. \qquad (10)$$

For Eu:KYbW, *R* = 12.1 which means a strong prevalence of the ED transition. This agrees with the assumption that Eu^{3+} ions in KYbW are located in C_2 sites without inversion center. The value of *R* for Eu:KYbW is similar to those for Eu:DTs (*R* = 10...13) [11,17,20]. In general, a large *R* value indicates an increase of the crystal field strength due to an increase in the covalence or in the distortion of the bonds surrounding the active ion. For Eu:DTs, large *R* values are related to (i) short average Eu–O distances in the Eu:KREW lattice (e.g., Yb–O distances are only 2.20–2.71 Å for the host crystal); (ii) high distortion of the EuO_8 environment (Δ_d ~4×10^{-3} for YbO_8 polyhedra).

The CIE 1931 (*Commission internationale de l'éclairage*) color coordinates for Eu: KYbW luminescence under UV excitation are *x* = 0.675 and *y* = 0.325 that fall into the red region. The dominant wavelength in the PL spectrum is 614 nm with 99% purity. These characteristics are close to those reported recently for bulk Eu:DTs, see Table 8. The CIE coordinates for the bulk Eu:KYbW agree with the results for nanocrystalline Eu:KYbW, x = 0.68 and y = 0.32 [24].

It should be noted that no sign of blue Eu^{2+} emission (which typically appears as a broad band centered at ~460 nm) was detected for Eu:KYbW crystals.

The polarized stimulated-emission (SE) cross-section spectra for Eu:KYbW were calculated with the Füchtbauer–Ladenburg equation [39]:

$$\sigma_{\mathrm{SE}}^{i}(\lambda) = \frac{\lambda^5}{8\pi n_i^2 \tau_{\mathrm{rad}} c} \frac{W_i(\lambda)}{1/3 \sum\limits_{i=p,m,g} \int \lambda W_i(\lambda) \mathrm{d}\lambda}. \qquad (11)$$

Here, $W_i(\lambda)$ is the measured spectral power density of luminescence for the principal polarization states, $E \parallel N_p$, N_m and N_g, π and σ oscillation states, λ is the light wavelength, n_i is the refractive index corresponding to *i*-th polarization, τ_{rad} is the radiative lifetime of the emitting state ($^5D_0$ level of Eu^{3+}), *c* is the speed of light. The results are shown in Fig. 6 for the $^5D_0 \rightarrow {}^7F_2$ and $^5D_0 \rightarrow {}^7F_4$ transitions which are of interest for laser operation. The detailed analysis of the SE cross-section spectra is shown in Table 9. As the $^5D_0$ state of Eu^{3+} has only one Stark sub-level, the high-resolution RT luminescence spectroscopy allowed us to determine the energy of the Stark sub-levels for $^7F_1$, $^7F_2$ and $^7F_4$ excited states, see Table 5.

The stimulated emission in the deep-red spectral region is determined by the $^5D_0 \rightarrow {}^7F_4$ transition. For light polarizations $E \parallel N_m$ and $E \parallel N_g$, the emission spectra contain two peaks at 703.2 and 706.4 nm ($\Gamma_1 \rightarrow \Gamma_2$). For $E \parallel N_p$, an intense peak at 705.0 nm is observed ($\Gamma_1 \rightarrow \Gamma_2$). The anisotropy of the peak SE cross-sections, $\sigma_{SE}(m)$: $\sigma_{SE}(p)$:$\sigma_{SE}(g)$, amounts to 5.5:1.3:1. The maximum σ_{SE} at 703.2 nm is 1.44×10^{-20} cm^2 (for $E \parallel N_m$). The SE in the red spectral region is determined by the $^5D_0 \rightarrow {}^7F_2$ transition. For $E \parallel N_m$ and $E \parallel N_g$, the spectra contain two peaks at 613.2 and 619.4 nm ($\Gamma_1 \rightarrow \Gamma_2$). For $E \parallel N_p$, the spectrum is also different containing two closely located peaks at 616.0 and 617.5 nm. The anisotropy of the cross-sections $\sigma_{SE}(m)$:$\sigma_{SE}(p)$:$\sigma_{SE}(g)$ for this band is less evident, 2.3:1.6:1. The maximum σ_{SE} at 613.2 nm is 4.21×10^{-20} cm^2 (for $E \parallel N_m$). Consequently, potential laser elements from Eu:KYbW should be cut so that they will provide access to the high-gain polarization $E \parallel N_m$ (i.e., N_p-cut or N_g-cut).

In Table 10, we have compared the SE cross-sections for Eu^{3+} ions when doped in the main representatives of the monoclinic DT family, KREW with RE = Gd, Y, Lu or Yb, showing that Eu:KYbW possesses the largest σ_{SE} for the $^5D_0 \rightarrow {}^7F_2$ transition.

Excited-state absorption (ESA) is an important issue limiting the performance of the rare-earth -based lasers. In the present paper, we calculated the absorption oscillator strengths *f* for the ESA from the metastable $^5D_0$ state of Eu^{3+}, Table 11. The mean wavelengths for these transitions were estimated from the energy of the higher-lying excited states of the Eu^{3+} freeion [37]. The strongest ESA processes are related to the $^5D_0 \rightarrow {}^5G_6$, $^5H_4$, $^5F_2$ and $^5F_4$ transitions. The mean wavelength of the $^5D_0 \rightarrow {}^5F_4$ super-intense ESA channel ($\langle\lambda\rangle$ ~611 nm) overlaps with an emission band of Eu^{3+} ions in KYbW related to the $^5D_0 \rightarrow {}^7F_2$ transition. The prediction of such an overlap for Eu^{3+}-doped materials was first reported in [40] for $EuAl_3(BO_3)_4$. The much weaker $^5D_0 \rightarrow {}^5H_6$ ESA transition ($\langle\lambda\rangle$ ~701 nm) may partially overlap with the emission band related to the $^5D_0 \rightarrow {}^7F_4$ transition. We expect that ESA limits the performance of Eu:KYbW red lasers.

4.3 Raman spectroscopy

Polarized Raman spectra of Eu:KYbW crystal for *p*(*xx*)*p*, *m*(*xx*)*m* and *g*(*xx*)*g* geometries are shown in Fig. 7. Here we use the standard notations, *a*(*bc*)*d*, where *a* and *d* represent the direction of excitation and registration, respectively, *b* and *c* are the polarization state of the excitation and scattered beams, respectively.

The phonons below 270 cm^{-1} are attributed to external lattice modes associated with translational motion of the cations of the structure (K^+, Yb^{3+}/Eu^{3+} and W^{6+}) and rotational motion of the WO_6 groups. The bending modes appear in the 270–460 cm^{-1} range, and the stretching modes - in the 400–1000 cm^{-1} range. The bands in the 430–750 cm^{-1} region which are not observed for scheelite-like crystals with isolated WO_4 tetrahedra, are related to double oxygen bridge vibrations. The spectra of Eu:KYbW are strongly polarized. The most intense stretching modes appear at 905.5 cm^{-1} (assigned as ν(W–O)/ν_1) and 756.0 cm^{-1} (ν(WOOW)*ν(W–O)/$\nu_3{}^0$). Here, W–O stands for tungsten-oxygen bonds, WOOW is the double oxygen bridge and * indicates the coupling of the vibrations. The linewidths (FWHM) of these lines are 10.4 and 15.9 cm^{-1}, respectively.

4.4 Discussion

In the present paper, we focus on the spectroscopic properties of Eu^{3+} ions in KYbW. The spectroscopy of Yb^{3+} ions for this stoichiometric material was described in detail in a previous work [27]. Here we just mention the main results. The maximum absorption cross section is $\sigma_{abs} = 11.7\times10^{-20}$ cm^2 at 981 nm (zero-line) with a linewidth of ~4 nm (for $E \parallel N_m$). The maximum SE cross-section is $\sigma_{abs} = 12.5\times10^{-20}$ cm^2 at zero-line and 2.5×10^{-20} cm^2 at 1024 nm (local peak in the gain spectra) for the same polarization. The experimental lifetime of Yb^{3+} in KYbW is ~200 μs (free-of-reabsorption value, measured with the powder method) and the radiative lifetime is ~270 μs.

Eu:KYbW is distinct from its monoclinic counterparts, Eu:KREW with RE = Gd, Y or Lu, as both Eu^{3+} and Yb^{3+} ions are optically active. The processes of energy transfer (ET) between them are possible which can be detected by variation of the experimental lifetimes of the emitting states. The upper laser level of Yb^{3+}, $^2F_{5/2}$, in KYbW is positioned at 10188–10734 cm^{-1} (in agreement with the Stark splitting). There are no states of Eu^{3+} in this energy range. However, it is known that for high Yb^{3+} concentrations, two adjacent Yb^{3+} ions can form a virtual excited state with energy $2E(^2F_{5/2})$. Such processes involving the virtual state are called cooperative ones [41,42]. For KYbW crystal, this virtual state of Yb^{3+} will have an energy of 20376–21468 cm^{-1}. Thus, direct or phonon-assisted (for KYbW, ν_{max} = 911 cm^{-1} [27]) ET from $^5D_1$ and $^5D_2$ states of Eu^{3+} to the virtual excited state of Yb^{3+}-Yb^{3+} pair is possible (and *vice versa*). The excitation of Eu:KYbW in the visible or UV may lead to the ~1 μm emission from Yb^{3+} ions. This process is known as cooperative down-conversion or "quantum cutting" [43] and it is especially efficient in stoichiometric materials [44]. The excitation of Yb^{3+} ions at ~1 μm may potentially lead to the visible (red) Eu^{3+} emission. This process is a cooperative up-conversion. Both of these processes were studied for Eu:KYbW [24,28,29]. We will just discuss their influence on the properties of Eu:KYbW as a potential laser crystal for Eu-lasers.

Previous measurements of PL decay from the $^5D_0$ state for Eu^{3+}-doped monoclinic DTs revealed that the measured decay time, τ_{exp}, is very close to the radiative lifetime, τ_{rad}, resulting in almost unity (>98%) luminescence quantum efficiency from this state [11,17,20]. This is in agreement with a very high energy gap for $^5D_0$ state to the lower lying excited-state $^7F_6$, ~12000 cm^{-1}, as compared with the maximum phonon frequency in DTs, ν_{max} ~903–907 cm^{-1}. Thus, almost zero non-radiative relaxation from the $^5D_0$ state is expected.

The PL decay curves for Eu:KYbW are shown in Fig. 8 (under excitation at 534 nm to the $^5D_1$ state). The measurement was performed for the $^5D_0 \rightarrow {}^7F_2$ (at ~610 nm) and $^5D_0 \rightarrow {}^7F_4$ (700 nm) transitions. The decay curves are clearly single-exponential. The luminescence decay time τ_{exp} equals 178±5 μs. Similar results are obtained under UV excitation at 355 nm (180±5 μs). The experimental lifetime of the $^5D_0$ state for Eu^{3+} ions in KYbW is shorter than the radiative one, resulting in a reduced luminescence quantum efficiency $\eta_q = \tau_{exp}/\tau_{rad}$ = 51%. The reason for this is the above mentioned ET between the Eu^{3+} ions and Yb^{3+}-Yb^{3+} ion pairs. This indicates that $KEu_xYb_{1-x}W$ compounds can be promising as down-conversion phosphors (when synthesized, e.g. in the nanocrystalline form). A second reason for the shortening of the

Eu^{3+} lifetime can be defects and impurities in the stoichiometric crystal which can be diminished by the growth of large-volume and highly uniform crystals similar to [17,20] and the use of higher purity Yb_2O_3 reagent. Previous measurements of $\tau_{exp}(^5D_0)$ for Eu:KYbW resulted in 227 μs for nanopowder [24] and 215 μs for bulk crystal [28].

Our studies of the luminescence decay of Yb^{3+} ions in Eu:KYbW (with the powder method, similarly to [27]) revealed no significant shortening of the experimental lifetime, τ_{exp} = 200±10 μs, as compared with that for pure KYbW. This indicates that the efficiency of cooperative up-conversion based on the $2Yb^{3+} \rightarrow Eu^{3+}$ ET is very small, estimated to be <2%. Indeed, the spectrum of up-conversion luminescence of Eu:KYbW crystal excited at 960 nm (to the $^2F_{5/2}$ Yb^{3+} state) contained mainly the emission bands from Er^{3+} and Tm^{3+} impurity ions in the green and blue which dominated over the red Eu^{3+} emission. Er and Tm are presented as impurities in the Yb_2O_3 reagent.

Further work on bulk Eu:KYbW should be focused on growth of large-volume crystals with high Eu^{3+} content (e.g., up to 20 at.%). It is known that the concentration-quenching in Eu:DTs is extremely weak even for high doping levels [11]. Thus, such samples can be suitable for laser operation. The growth of crystals along the [001] direction can also be useful for orientation of the laser elements along the N_g-axis which is beneficial to access the high absorption and SE cross-sections (see Fig. 3 and Fig. 6), as well as good thermo-optic properties [14].

5. Conclusion

We report on the growth and a detailed spectroscopic study of monoclinic 1 at.% Eu:KYbW crystal. The polarized RT absorption spectra were measured revealing the suitability of pumping the Eu:KYbW crystal into the $^7F_1 \rightarrow {}^5D_1$ band peaked at 534.2 nm with $\sigma_{abs} = 1.32\times10^{-20}$ cm^2 and bandwidth of 0.7 nm. The polarized low- temperature (6 K) absorption and RT high-resolution emission studies allowed us to determine the Stark splitting of the ^7F_J, ^5D_J and $^5L_6$ multiplets of Eu^{3+}. It was found that the modification of the Judd-Ofelt theory for the case of a strong configuration interaction (SCI) was very suitable for the description of Eu^{3+} ions in KYbW. With the J-O modeling, the probability of spontaneous transitions, radiative lifetimes and luminescence branching ratios were determined. For Eu:KYbW, the maximum stimulated-emission cross-section corresponding to the $^7F_1 \rightarrow {}^5D_1$ transition was 1.44×10^{-20} cm^2 at 703.2 nm. Eu:KYbW is promising for deep-red lasers at ~703 nm and red phosphors (CIE 1931 coordinates, x = 0.675, y = 0.325). Laser operation with Eu:KYbW is expected with large-volume and highly-doped (~20 at.%) crystals.

Acknowledgements

This work was supported by the Spanish Government under projects MAT2013-47395-C4-4-R and TEC2014-55948-R, and by the Generalitat de Catalunya under project 2014SGR1358. F.D. acknowledges additional support through the ICREA academia award 2010ICREA-02 for excellence in research. This work is part of a project that has received funding from the European Union's Horizon 2020 research and innovation programme under the Marie Skłodowska-Curie grant agreement No 657630.

References

1. P.W. Metz, F. Reichert, F. Moglia, S. Müller, D.-T. Marzahl, C. Kränkel, G. Huber, Opt. Lett. 39 (2014) 3193-3196.
2. M. Fibrich, H. Jelínková, J. Šulc, K. Nejezchleb, V. Škoda, Appl. Phys. B 97 (2009) 363.
3. P.W. Metz, S. Müller, F. Reichert, D.-T. Marzahl, F. Moglia, C. Kränkel, G. Huber, Opt. Express 21 (2013) 31274-31281.
4. A. Richter, E. Heumann, G. Huber, V. Ostroumov, W. Seelert, Opt. Express 15 (2007) 5172-5178.
5. D.-T. Marzahl, P. W. Metz, C. Kränkel, G. Huber, Opt. Express, 23 (2015) 21118-21127.
6. G. Bolognesi, D. Parisi, D. Calonico, G.A. Costanzo, F. Levi, P.W. Metz, C. Kränkel, G. Huber, M. Tonelli, Opt. Lett. 39 (2014) 6628–6631.
7. G. Wakefield, E. Holland, P.J. Dobson, J.L. Hutchison, Adv. Mater. 13 (2001) 1557–1560.
8. E.J. Schimitschek, Appl. Phys. Lett. 3 (1963) 117–118.
9. N.C. Chang, J. Appl. Phys. 34 (1963) 3500–3504.
10. S.N. Bagaev, V.I. Dashkevich, V.A. Orlovich, S.M. Vatnik, A.A. Pavlyuk, A.M. Yurkin, Quantum Electron. 41 (2011) 189–192.
11. P.A. Loiko, V.I. Dashkevich, S.N. Bagaev, V.A. Orlovich, A.S. Yasukevich, K.V. Yumashev, N.V. Kuleshov, E.B. Dunina, A.A. Kornienko, S.M. Vatnik, A.A. Pavlyuk, Laser Phys. 23 (2013) 105811-1-7.
12. V. Petrov, M.C. Pujol, X. Mateos, O. Silvestre, S. Rivier, M. Aguilo, R.M. Sole, J. Liu, U. Griebner, F. Diaz, Laser & Photon. Rev. 1 (2007) 179–212.
13. J. Liu, V. Petrov, X. Mateos, H. Zhang, J. Wang, Opt. Lett. 32 (2007) 2016–2018.
14. J. M. Serres, X. Mateos, P. Loiko, K. Yumashev, N. Kuleshov, V. Petrov, U. Griebner, M. Aguiló, and F. Díaz, Opt. Lett. 39 (2014) 4247-4250.
15. P. Loiko, J.M. Serres, X. Mateos, K. Yumashev, N. Kuleshov, V. Petrov, U. Griebner, M. Aguiló, F. Díaz, Opt. Lett. 40 (2015) 344–347.
16. M.C. Pujol, J.J. Carvajal, X. Mateos, R. Sole, J. Massons, M. Aguilo, F.Diaz, J. Lumin. 138 (2013) 77–82.
17. P.A. Loiko, V.I. Dashkevich, S.N. Bagaev, V.A. Orlovich, A.S. Yasukevich, K.V. Yumashev, N.V. Kuleshov, E.B. Dunina, A.A. Kornienko, S.M. Vatnik, A.A. Pavlyuk, J. Lumin. 153 (2014) 221–226.
18. V.I. Dashkevich, S.N. Bagaev, V.A. Orlovich, A.A. Bui, P.A. Loiko, K.V. Yumashev, N.V. Kuleshov, S.M. Vatnik, A.A. Pavlyuk, Laser Phys. Lett. 12 (2015) 015006-1-6.
19. V.I. Dashkevich, S.N. Bagayev, V.A. Orlovich, A.A. Bui, P.A. Loiko, K.V. Yumashev, A.S. Yasukevich, N.V. Kuleshov, S.M. Vatnik, A.A. Pavlyuk, Laser Phys. Lett. 12 (2015) 085001-1-5.
20. P.A. Loiko, V.I. Dashkevich, S.N. Bagaev, V.A. Orlovich, X. Mateos, J.M. Serres, E.V. Vilejshikova, A.S. Yasukevich, K.V. Yumashev, N.V. Kuleshov, E.B. Dunina, A.A. Kornienko, S.M. Vatnik and A.A. Pavlyuk, J. Lumin. 168 (2015) 102–108.
21. T.Koubaa, M.Dammak, M.C.Pujol, M.Aguiló, F.Díaz, J. Lumin. 168 (2015) 7–13.
22. R. Pazik, A. Zych, W. Strek, Mater. Chem. Phys. 115 (2010) 536–540.

23. L. Macalik L, P.E. Tomaszewski, R. Lisiecki, J. Hanuza J. Sol. State Chem. 131 (2008) 2591–2600.
24. M. Galceran, M.C. Pujol, P. Gluchowski, W. Strek, J.J. Carvajal, X. Mateos, M. Aguilo, F. Diaz, Opt. Mater. 32 (2010) 1493–1500.
25. A. Lukowiak, R.J. Wiglusz, R. Pazik, K. Lemanski, W. Strek, J. Rare Earth 27 (2008) 564–568.
26. X. Gao, Y. Wang, D. Wang, B. Liu, J. Lumin. 129 (2009) 840–843.
27. M.C. Pujol, M.A. Bursukova, F. Guell, X. Mateos, R. Sole, Jna. Gavalda, M. Aguilo, J. Massons, F. Diaz, P. Klopp, U. Griebner, V. Petrov, Phys. Rev. B 65 (2002) 165121-1-11.
28. W. Strek, P.J. Deren, A. Bednarkiewicz, Y. Kalisky, P. Boulanger, J. Alloys Cmpnd. 300–301 (2000) 180–183.
29. W. Strek, P.J. Deren, A. Bednarkiewicz J. Lumin. 87–89 (2000) 999–1001.
30. B.R. Judd, Phys. Rev. 172 (1962) 750–761.
31. G.S. Ofelt, J. Chem. Phys. 37 (1962) 511–519.
32. E.B. Dunina, A.A. Kornienko, L.A. Fomicheva, Cent. Eur. J. Phys. 6 (2008) 407–414.
33. A.A. Kornienko, E.B. Dunina, V.L. Yankevich, Opt. Spectr. 81 (1996) 871–874.
34. E.B. Dunina, A.A. Kornienko, Opt. Spectr. 116 (2014) 706–711.
35. C. Görller-Walrand, K. Binnemans, “Rationalization of crystal – field parameterization,” Hand book on the physics and chemistry of rare earths, Elsevier, 121- 283 (1996).
36. C.M. Dodson, R. Zia, Phys. Rev. B 86 (2012) 125102-1-10.
37. W. T. Carnall, P. R. Fields, K. Rajnak, J. Chem. Phys. 49 (1968) 4450.
38. A.F. Kirby, F.S. Richardson, J. Phys. Chem. 87 (1983) 2544–2556.
39. B.F. Aull, H.P. Jenssen, IEEE J. Quantum Electron. 18 (1982) 925–930.
40. G.E. Malashkevich, A.A. Kornienko, E.B. Dunina, V.N. Sigaev, N.V. Golubev, E.H. Mamadjanova, A. Paleary, J. Appl. Spectr. 80 (2013) 536–541.
41. Y. Dwivedi, S.N. Thakur, S.B. Rai, Appl. Phys. B 89 (2007) 45–51.
42. P.A. Loiko, G.E. Rachkovskaya, G.B. Zakharevich, A.A. Kornienko, E.B. Dunina, A.S. Yasukevich, K.V. Yumashev, J. Non-Cryst. Solids. 392-393 (2014) 39-44.
43. J. T. van Wijngaarden, S. Scheidelaar, T. J. H. Vlugt, M. F. Reid, A. Meijerink, Phys. Rev. B 81 (2010) 155112-1–6.
44. P.A. Loiko, N.M. Khaidukov, J. Méndez-Ramos, E.V. Vilejshikova, N.A. Skoptsov, K.V. Yumashev, J. Lumin. 170 (2016) 1–7.

Figure captions

Figure 1. Image of the as-grown Eu:KYbW crystal, the [010] axis is pointing towards the observer.

Figure 2. Measured optical absorption spectrum of Eu:KYbW (RT, light polarization $E \parallel N_m$).

Figure 3. Polarized RT absorption bands related to the $^7F_{0,1} \rightarrow {}^5L_6$ (a), $^7F_0 \rightarrow {}^5D_2$ (b) and $^7F_{0,1} \rightarrow {}^5D_1$ (c) transitions of Eu^{3+} ions in KYbW.

Figure 4. Polarized absorption bands of Eu^{3+} ions in KYbW at 6 K, "+" denotes peaks taken into account for the determination of the Stark levels.

Figure 5. Photoluminescence (PL) spectrum of Eu:KYbW (at RT, non-polarized emission, the excitation wavelength is 405 nm, J → J' notations correspond to $^5D_J \rightarrow {}^7F_{J'}$ transitions).

Figure 6. Polarized stimulated-emission cross-section, σ_{SE}, spectra corresponding to the $^5D_0 \rightarrow {}^7F_2$ (a) and $^5D_0 \rightarrow {}^7F_4$ (b) transitions, for Eu:KYbW (at RT).

Figure 7. Polarized Raman spectra of Eu:KYbW for the *p*(*xx*)*p* (a), *m*(*xx*)*m* (b) and *g*(*xx*)*g* (c) geometries. The excitation wavelength is 632.8 nm.

Figure 8. Decay of the red luminescence of Eu^{3+} ions at 610 nm (a) and 702 nm (b) for Eu:KYbW. The excitation wavelength is 534 nm.

Figure 1

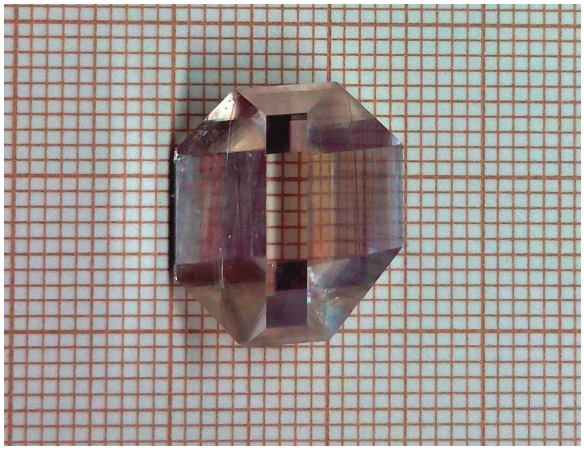

Figure 2

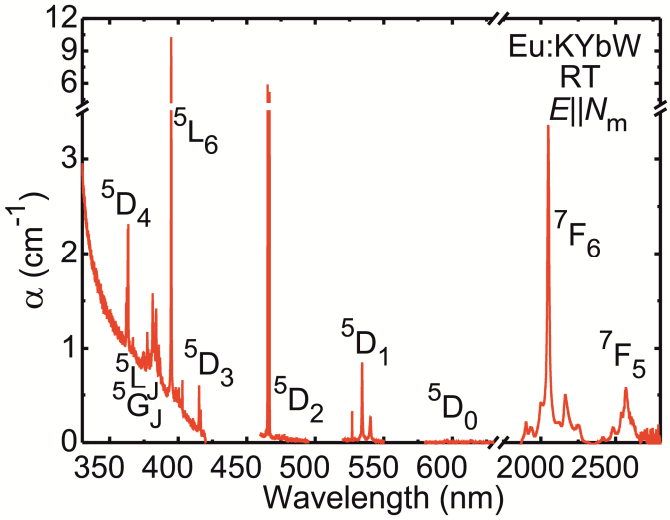

Figure 3

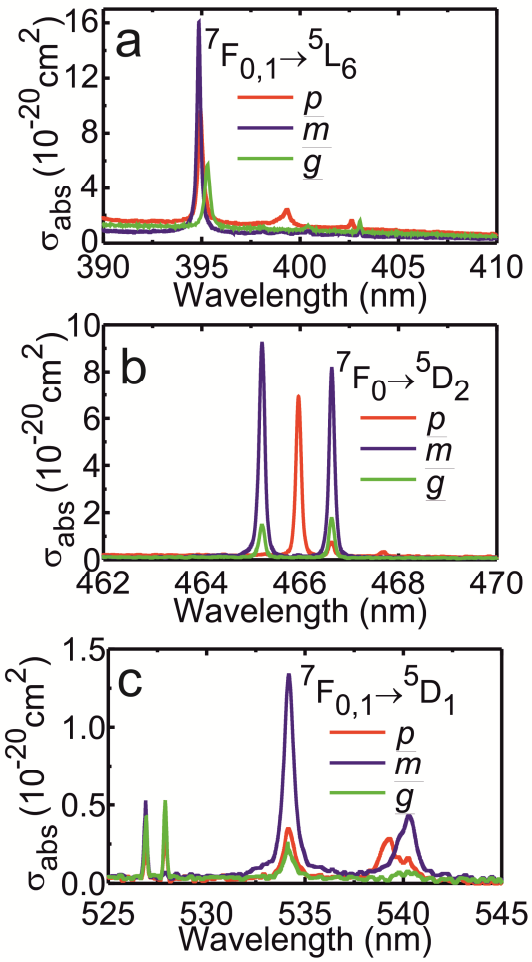
a
$^7F_{0,1}\rightarrow{}^5L_6$
p
m
g
σ_{abs} (10^{-20}cm^2)
Wavelength (nm)
b
$^7F_0\rightarrow{}^5D_2$
c
$^7F_{0,1}\rightarrow{}^5D_1$

Figure 4

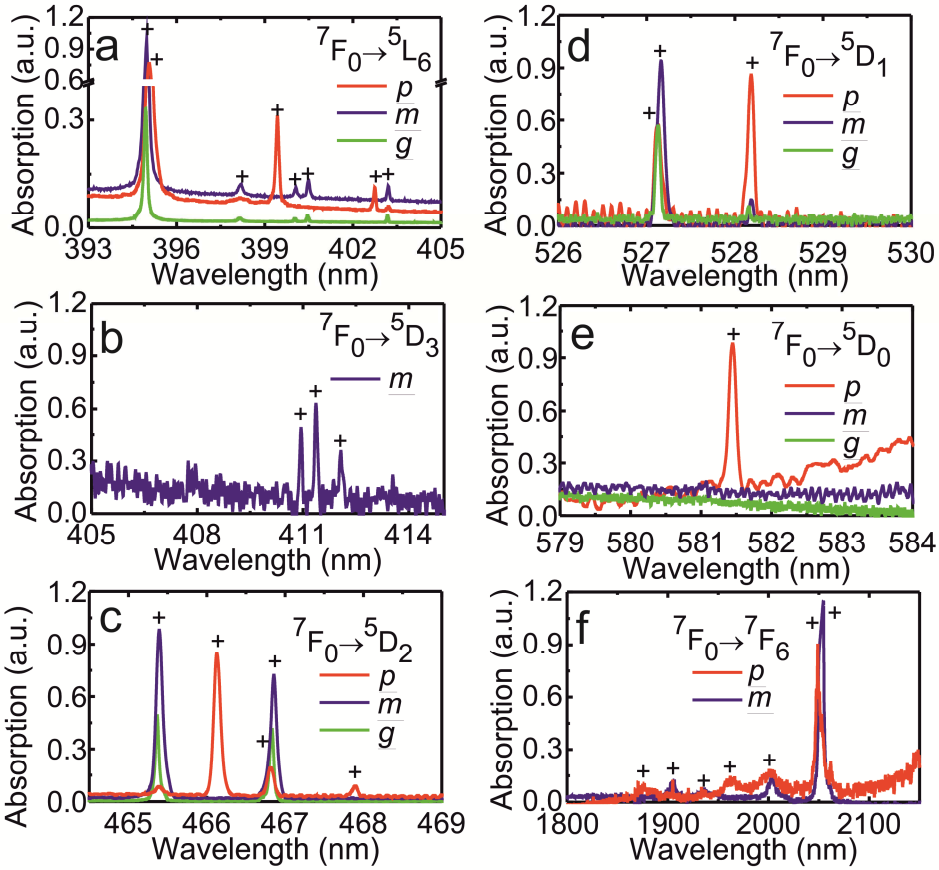

Figure 5

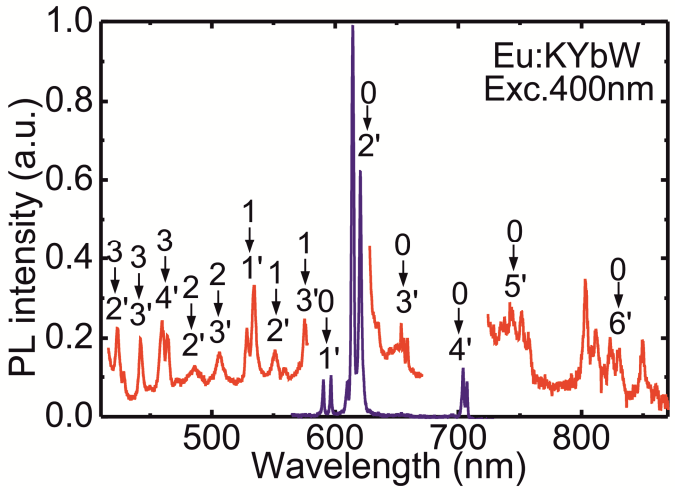

Figure 6

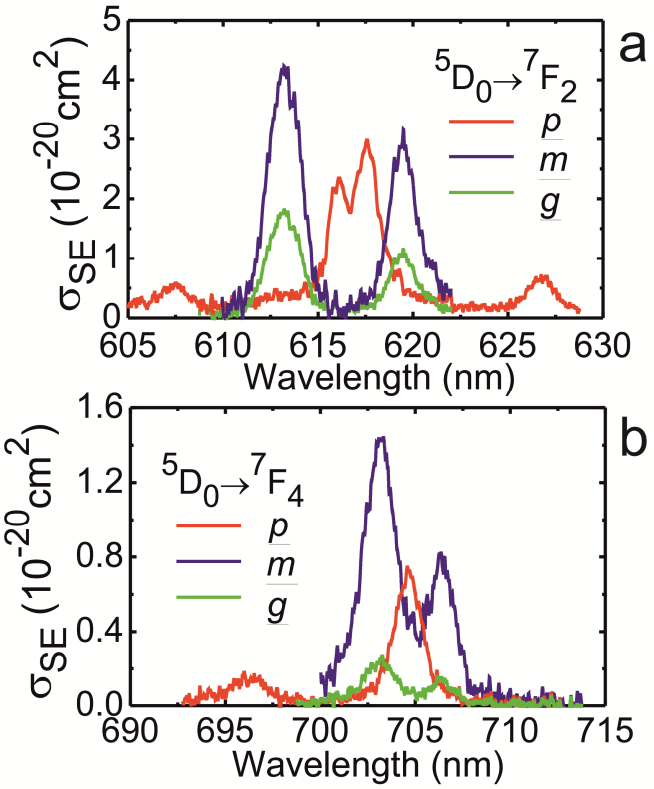

Figure 7

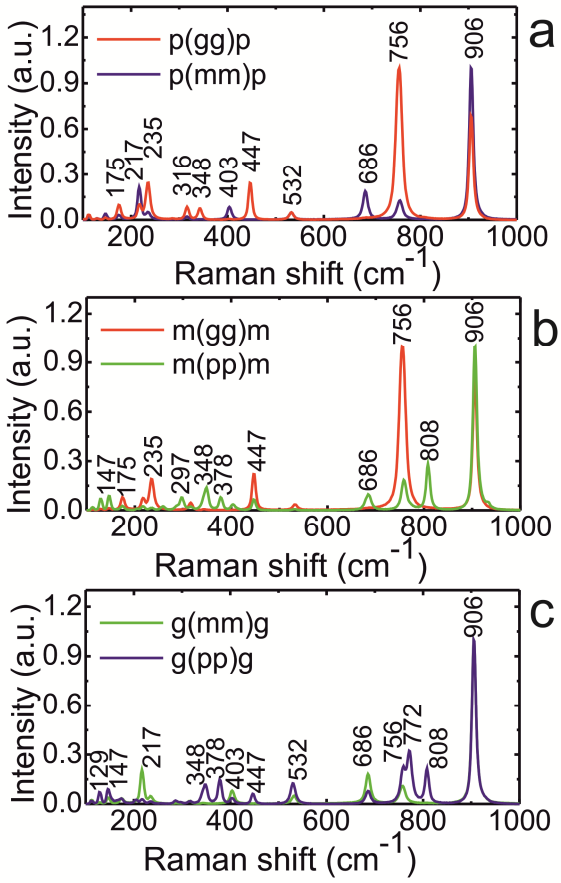

Figure 8

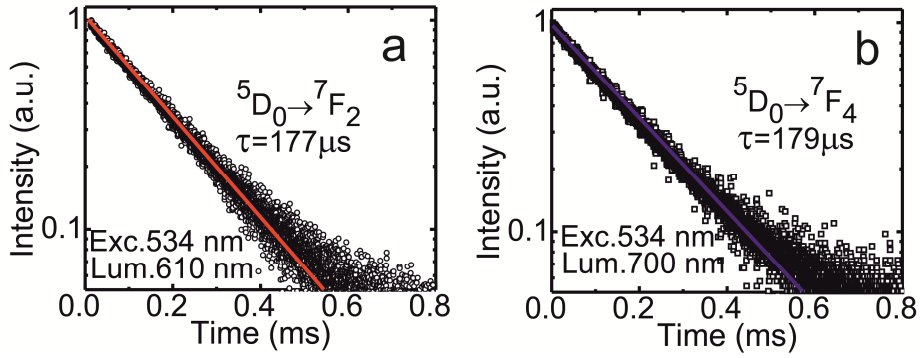
a
$^5D_0 \rightarrow {}^7F_2$
τ=177μs
Exc.534 nm
Lum.610 nm
Intensity (a.u.)
Time (ms)
b
$^5D_0 \rightarrow {}^7F_4$
τ=179μs
Exc.534 nm
Lum.700 nm
Intensity (a.u.)
Time (ms)